# Ion-Exchangeable, Electronically Conducting Layered Perovskite Oxyfluorides

**ARTICLE** *in* JOURNAL OF THE AMERICAN CHEMICAL SOCIETY · JULY 2009

Impact Factor: 12.11 · DOI: 10.1021/ja9040829 · Source: PubMed

J|A|C|S ARTICLES

Published on Web 06/23/2009

# Ion-Exchangeable, Electronically Conducting Layered Perovskite Oxyfluorides

Yoji Kobayashi,[†] Mingliang Tian,[‡] Miharu Eguchi,[†] and Thomas E. Mallouk*,[†]

*Departments of Chemistry and Physics, The Pennsylvania State University, University Park, Pennsylvania 16802*

Received May 19, 2009; E-mail: tom@chem.psu.edu

***Abstract:*** Cation-exchangeable $d^0$ layered perovskites are amenable to intercalation, exfoliation, and a variety of topochemical reactions, but they lack the interesting electronic and magnetic functionalities of mixed-valent perovskites. Conversely, electronically and magnetically interesting layered perovskites lack scope in terms of interlayer chemistry. To bridge this gap, the insulating, cation-exchangeable layered perovskites $RbLaNb_2O_7$, $KCa_2Nb_3O_{10}$, and $NaYTiO_4$ were reacted with poly(tetrafluoroethylene) under inert atmosphere conditions to yield layer perovskites in which some of the oxygen is substituted by fluorine. In the fluorinated materials, the B-site cations are reduced to a mixed-valent state without introducing oxygen vacancies into the anion sublattice. The resulting electronically conducting solids can be exposed to air and water and even ion-exchanged in acid without oxidation of the B-site cations. Electronic transport measurements on the air-stable $RbLaNb_2O_6F$ reveal room-temperature conductivity ($2-7 \times 10^2$ $\Omega\cdot$cm) via a variable-range hopping mechanism, which is not substantially changed after aqueous proton exchange to $H_{1-x}Rb_xLaNb_2O_6F$ ($x \approx 0.2$).

## Introduction

Layered perovskites can have a number of interesting electronic properties, including superconductivity[1,2] and colossal magnetic resistance,[3,4] that entail doping and mixed valency. However, mixed-valent layered perovskites and related layered oxides are ordinarily not ion-exchangeable for two reasons. First, if the charge on the B-site transition metal ion is low (e.g., $Cu^{2+}$ or $Mn^{3+}$), then multiply charged interlayer ions are needed to balance the charge of the anion lattice. Second, the compound can be susceptible to unwanted side reactions, such as hydrolysis or oxidation−reduction in the aqueous media that are used to carry out the ion-exchange reaction.

Ion-exchangeable layered solids are useful building blocks for designed materials and thin films because they are amenable to a wide range of intercalation and exfoliation reactions.[5−8] Topochemical reactions have been developed to interconvert the structural families of ion-exchangeable layer perovskites, and it is possible to grow arbitrary sequences of layers as thin films.[6] One common feature of ion-exchangeable perovskites is that they contain $d^0$ early transition metal B-site cations (such as $Ti^{4+}$, $Nb^{5+}$, $Ta^{5+}$). These compounds contain exchangeable interlayer cations but are typically wide band gap (3−4 eV) insulators and thus do not have interesting electronic or magnetic properties themselves. Some exceptions are perovskites that contain rare earths to induce photoluminescence,[9,10] transition metal ions such as Mn to impart magnetism,[11] or nitrogen on oxygen lattice sites to narrow the band gap.[12]

Reduced early transition metal perovskites are known; however, these compounds have been typically obtained by reduction and insertion of an alkali metal into the interlayer, as in $(Li_xVO)La_2Ti_3O_{10}$,[15] $Na_{2-x+y}Ca_{x/2}La_2Ti_3O_{10}$,[16] $Na_{1-x+y}Ca_{x/2}LaTiO_4$,[17] $(Li_xCl)LaNb_2O_7$,[18] $Rb_2LaNb_2O_7$,[19] and other layered tantalates.[20] All of these materials are at least moderately air sensitive. Furthermore, as the mixed valence is induced

[†] Department of Chemistry.
[‡] Department of Physics.

(1) Enz, C. P. *Lect. Notes Phys.* **1996**, *477*, 143–160.
(2) Bednorz, J. G.; Müller, K. A. *Z. Phys. B: Condens. Matter* **1986**, *64*, 189–193.
(3) Mitchell, J. F.; Millburn, J. F.; Medarde, M.; Short, S.; Jorgensen, J. D.; Fernandez-Diaz, M. T. *J. Solid State Chem.* **1998**, *141*, 599–603.
(4) Argyriou, D. N.; Mitchell, J. F.; Potter, C. D.; Bader, S. D.; Kleb, R.; Jorgensen, J. D. *Phys. Rev. B* **1997**, *55*, 11965–11968.
(5) Schaak, R. E.; Mallouk, T. E. *Chem. Mater.* **2000**, *12*, 2513–2516.
(6) Schaak, R. E.; Mallouk, T. E. *Chem. Mater.* **2002**, *14*, 1455–1471.
(7) Ma, R.; Bando, Y.; Sasaki, T. *J. Phys. Chem. B* **2004**, *108*, 2115–2119.
(8) Takagaki, A.; Yoshida, T.; Lu, D.; Kondo, J. N.; Hara, M.; Domen, K.; Hayashi, S. *J. Phys. Chem. B* **2004**, *108*, 11549–11555.
(9) Ida, S.; Ogata, C.; Unal, U.; Izawa, K.; Inoue, T.; Altuntasoglu, O.; Matsumoto, Y. *J. Am. Chem. Soc.* **2007**, *129*, 8956–8957.
(10) Kudo, A.; Sakata, T. *J. Phys. Chem.* **1995**, *99*, 15963–15967.
(11) Schaak, R. E.; Afzal, D.; Schottenfeld, J. A.; Mallouk, T. E. *Chem. Mater.* **2002**, *14*, 442–448.
(12) Schottenfeld, J. A.; Benesi, A. J.; Stephens, P. W.; Chen, G.; Eklund, P. C.; Mallouk, T. E. *J. Solid State Chem.* **2005**, *178*, 2313–2321.
(13) Hase, I.; Nishihara, Y. *Phys. Rev. B* **1998**, *58*, 1707–1709.
(14) Tobias, G.; Canadell, E. *J. Am. Chem. Soc.* **2006**, *128*, 4318–4329.
(15) Neiner, D.; Sweany, R. L.; Golub, V.; Wiley, J. B. *J. Mater. Chem.* **2006**, *16*, 186–191.
(16) Lalena, J. N.; Cushing, B. L.; Falster, A. U.; Simmons, W. B.; Seip, C. T.; Carpenter, E. E.; O'Connor, C. J.; Wiley, J. B. *Inorg. Chem.* **1998**, *37*, 4484–4485.
(17) Mcintyre, R. A.; Falster, A. U.; Li, S.; Simmons, W. B. J.; O'Connnor, C. J.; Wiley, J. B. *J. Am. Chem. Soc.* **1998**, *120*, 217–218.
(18) Viciu, L.; Kodenkandath, T. A.; Wiley, J. B. *J. Solid State Chem.* **2007**, *180*, 583–588.
(19) Armstrong, A. R.; Anderson, P. A. *Inorg. Chem.* **1994**, *33*, 4366–4369.
(20) Toda, K.; Masaki, T.; Teranishi, T.; Ye, Z.-G.; Sato, M.; Hinatsu, Y. *J. Mater. Chem.* **1999**, *9*, 799–803.

  

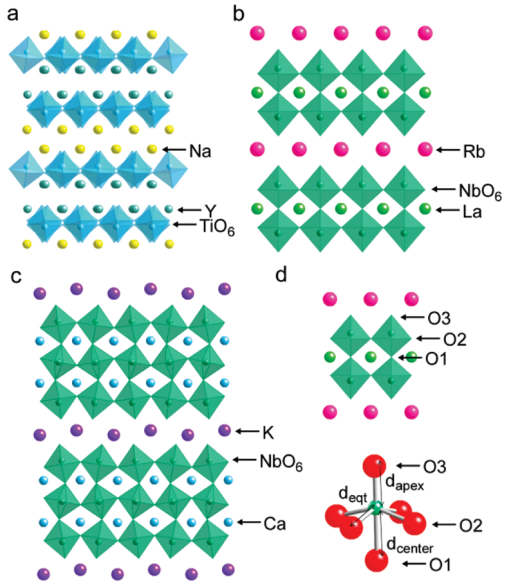


***Figure 1.*** Structures of (a) $NaYTiO_4$, (b) $RbLaNb_2O_7$, (c) $KCa_2Nb_3O_{10}$, and (d) the three different oxygen sites in $RbLaNb_2O_7$.

by changes in the composition of the interlayer gallery, ion exchange or exfoliation can cause the sheets to re-oxidize and lose their interesting electronic properties.

Here, we explore the reductive fluorination of ion-exchangeable Dion−Jacobson and Ruddlesden−Popper layered perovskites to obtain mixed-valence compounds that, potentially, could be exfoliated into single-layer sheets. Electronic structure calculations have shown that layer perovskites can become 2D metals if an extra electron is injected into the conduction band via reduction.[13,14] If the mixed-valence state is reasonably stable in air, such a finding would provide an interesting parallel to graphene sheets and provide a whole new class of electronically conducting oxide nanosheets.

An alternative to modifying the interlayer is reduction by chemically doping the octahedral lattice of the peroskite sheets themselves. There are reports of manipulating the A-site cations by high-temperature solid-state reations to create mixed-valent perovskites.[21,22] In this study we explore a relatively low temperature reaction that does not depend on special redox properties of the A-site cations and may thus be applicable to a broader range of layered oxides. We report a reductive fluorination reaction that yields the air-stable mixed-valence oxyfluoride $RbLaNb_2O_6F$ and its $n = 3$, 1 analogues $KCa_2Nb_3O_{9-x}F_x$ and $NaYTiO_{4-x}F_x$ ($n$ corresponds to the number of linked octahedra in the direction of the stacking axis). $RbLaNb_2O_6F$ undergoes cation exchange in aqueous acid without loss of lattice fluoride or electronic conductivity.

The structures of the layer perovskites used in this study are shown in Figure 1. These compounds differ in the number of $MO_6$ octahedra ($n = 1-3$) forming each perovskite block. It is typical of the $MO_6$ octahedra to be slightly distorted, especially for $NbO_6$ with shorter Nb−O bond lengths toward the interlayer, as shown in the Figure 1b. The interlayer alkali cations are exchangeable, and in the case of $RbLaNb_2O_7$ and $KCa_2Nb_3O_{10}$, the exchange reaction with protons followed by low-charge-density bases (alkylamines or tetra(*n*-butylammonium) hydroxide) can be used to exfoliate the sheets. The $n = 1$ Ruddlesden−Popper phase $NaYTiO_4$ is not known to exfoliate.

When the fluorine is exchanged for oxygen, it has a choice between a number of crystallographic sites. In $RbLaNb_2O_7$, there are crystallographically distinct central, equatorial, and apical oxygen sites in the $NbO_6$ octahedra (see Figure 1d). The multiplicities of these sites are 1, 4, and 2; so, in addition to energetics, statistical factors may also come into play in determining the fluorine positions in partially fluorinated structures.

We investigated both poly(vinylidene fluoride) (PVDF, monomer unit $CH_2CF_2$) and poly(tetrafluoroethylene) (PTFE, monomer unit $CF_2$) as possible fluorinating agents. Here, the carbon in the fluoropolymer acts as a reducing agent, ideally leaving the system as $CO_2$. A possible reaction of $RbLaNb_2O_7$ and PTFE under an inert atmosphere is shown below:

$$2RbLaNb_2O_7 + CF_2 \rightarrow 2RbLaNb_2O_6F + CO_2$$

The use of PVDF in the synthesis of the oxyfluorides $Sr_2TiO_3F_2$,[23] $Ca_2CuO_2F_2$,[23] and $SrFeO_2F$[24] was introduced by Slater and co-workers. The stoichiometry of PVDF reduction, however, makes a wider range of reactions and products possible, including a carbon residue:

$$2RbLaNb_2O_7 + CH_2CF_2 \rightarrow 2RbLaNb_2O_6F + C + H_2O + CO$$

Consistent with the stoichiometry of these reactions, we find significantly less carbon impurity in the fluorinated products made by the PTFE route.

## Experimental Section

$RbLaNb_2O_7$ was prepared by heating $Rb_2CO_3$ (25% excess), $La_2O_3$ (pre-treated at 900 °C for 24 h), and $Nb_2O_5$ at 850 °C for 30 min and then at 1100 °C for 2 days. $NaYTiO_4$ was prepared by heating $Na_2CO_3$ (20% excess), $Y_2O_3$, and $TiO_2$ at 900 °C for 1 day, while $KCa_2Nb_3O_{10}$ was prepared by mixing $K_2CO_3$ (10% excess), $CaCO_3$, and $Nb_2O_5$ and heating at 1200 °C for 10 h. After cooling, the solid reaction products were washed with water 2−3 times to ensure no excess alkali species remained.

Fluorination reactions were typically carried out by intimately mixing 0.5 g of the layer perovskite with 1.2 or 0.6 equvi of either poly(vinylidene fluoride) (PVDF, Alfa Aesar) or poly(tetrafluoroethylene) (PTFE, Sigma-Aldrich, 1 $\mu$m powder) under ethanol (1 equiv is defined as the amount required by stoichiometry to obtain $RbLaNb_2O_6F$ from $RbLaNb_2O_7$). The solid mixtures were pressed into 13 mm pellets, loaded into a passivated copper boat, and heated to 400 °C for 12 h at 10 °C/min under flowing nitrogen. In most cases, a second or third fluorination was conducted by grinding the pellets with additional fluoropolymer, pelletizing, and heating at the same conditions. The near-black samples had no detectable color change over a period of a few weeks. Control reactions between $RbLaNb_2O_7$ and polyethylene powder or activated carbon were performed by preparing pellets in the same way, using an amount of carbon that was the same as in a run with PTFE or PVDF.

$RbLaNb_2O_6F$ was proton-exchanged by shaking 1.0 g of $RbLaNb_2O_6F$ (prepared by three 0.6 equiv fluorinations using PTFE) in 50 mL of 2 M hydrochloric or nitric acid. The exchange reaction was carried out for 1, 3, or 5 days with daily centrifugation and renewal of the acid solution. After the final exchange/centrifugation step, samples were washed with water (three times) and ethanol

(21) Hamada, D.; Machida, M.; Sugahara, Y.; Kuroda, K. *J. Mater. Chem.* **1996**, *6*, 69–72.
(22) Sugimoto, W.; Ohkawa, H.; Naito, M.; Sugahara, Y.; Kuroda, K. *J. Solid State Chem.* **1999**, *148*, 508–512.
(23) Slater, P. R. *J. Fluorine Chem.* **2002**, *117*, 43–45.
(24) Berry, F. J.; Ren, X.; Heap, R.; Slater, P. R.; Thomas, M. F. *Solid State Commun.* **2005**, *134*, 621–624.

(twice) before drying under vacuum for 12 h. Further intercalation was conducted by dispersing 110 mg of $HLaNb_2O_6F$ (the 5-day ion exchange product with nitric acid) in 25 mL of degassed THF; 1 mL of propylamine (~60 equiv) was added, and the suspension was stirred for 4 days before the solvent and excess propylamine were removed *in vacuo*. One gram of $KCa_2Nb_3O_{10-x}F_x$ was proton-exchanged with 25 mL of 2 M nitric acid, which was replaced daily for 5 days; propylamine was intercalated into the protonated product (100 mg) by stirring in a mixture of THF/propylamine (9 mL, 1 mL; ~60 equiv).

X-ray diffraction patterns were obtained using Cu $K\alpha_1$ radiation on a Scintag Pad V diffractometer or Philips X'pert MPD system operating in Bragg−Brentano geometry. For lattice parameter refinement and Rietveld analysis, silicon powder was added as an internal standard. Data for Rietveld refinement were acquired by scanning from 5 to 90° with a step scan of 0.015° and a count time of 2.5 s. Rietveld analysis was conducted using the GSAS package[25] with the EXPGUI interface.[26]

Elemental analyses for fluorine and carbon were conducted by Galbraith Analytical Laboratories (Knoxville, TN) and Atlantic Microlab (Norcross, GA). Fluorine analysis was performed by Atlantic Microlab by oxygen flask combustion followed by ion chromatography. Galbraith Analytical Laboratories performed fluorine analysis by oxygen flask combustion followed by determination with a fluoride ion selective electrode. Results from the two analytical methods were consistent within 5−10%. The carbon content of samples was determined by CHN combustion analysis at Atlantic Microlabs. Transmission electron microscopy studies were conducted using either a JEOL-2010 $LaB_6$ (200 kV) or JEOL-2010F (200 kV) electron microscope. Electronic structure calculations were carried out using the generalized gradient approximation (GGA) exchange correlation and the full-potential linearized augmented plane wave (FLAPW) method as implemented in the WIEN2k package.[27] A total of 300 *k*-points gave reasonable convergence for the insulating parent oxide and metallic products; non-spin-polarized calculations were performed using the total energy as the convergence criterion. Structural data were entered as obtained from Rietveld refinement results, without further optimization. For the fluorinated products, supercell calculations were costly, and hence a virtual crystal approximation (VCA) was adopted. This entails using a pseudoatom which has averaged properties between fluorine and oxygen (for example, it may have an atomic number of 8.5) and placing it at the appropriate oxygen lattice sites.

## Results and Discussion

**Reactivity and Chemical Analysis.** All three of the oxide layer perovskites are white compounds, but upon reaction with PTFE, they turn dark gray-black. This change in color is somewhat expected, as the lanthanum niobate perovskites $RbLaNb_2O_7$ and $HLaNb_2O_7$ also become blue-black after reduction with hydrogen at elevated temperatures.[28] The reduced perovskites are expected to be $d^0-d^1$ mixed-valence compounds with a slightly populated $t_{2g}$ conduction band. Intraband transitions result in a black color, as is the case in many reduced transition metal oxides. In the case of the hydrogen-reduced samples, the bluish tint is from the intervalence charge-transfer absorption centered at ~1100 nm.

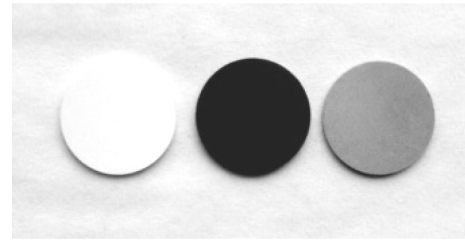

***Figure 2.*** Pellets of $RbLaNb_2O_7$, $RbLaN_2O_7$ after reaction with PTFE, and $RbLaN_2O_7$ mixed with 1 wt % graphite.

While the fluorinated products of the $NaYTiO_4$, $RbLaNb_2O_7$, and $KCa_2Nb_3O_{10}$ reactions have the characteristic black color of reduced perovskites, it is important to determine whether the reduction is accompanied by fluorine exchange for oxygen. A black color could also result from simple carbothermal reduction (i.e., the formation of $RbLaNb_2O_{6.5}$ rather than $RbLaNb_2O_6F$, for example) or even from carbonaceous impurities. Figure 2 illustrates that carbon impurities alone cannot cause this dramatic color change. The image compares the colors of pellets of pristine $RbLaNb_2O_7$, a pellet after reaction with PTFE, and a pellet of $RbLaNb_2O_7$ that contains the same amount (~1 wt %) of carbon in the form of graphite.

The possibility of a carbothermal reduction was investigated by heating $RbLaNb_2O_7$ with polyethylene or activated carbon such that the amount of carbon added was the same as in the PVDF or PTFE samples. The X-ray diffraction patterns in Figure 3 show a structural change only when a fluoropolymer is used; that is, the 001 peak at 8° has shifted to lower angle (see Figure 3b), and the previously overlapping peaks near 32.5° have also shifted to reveal three peaks (110, 004, and 111 reflections; see Figure 3a,b). After reaction, the products treated with polyethylene and activated carbon were only a light to medium gray, as opposed to the almost black PTFE/PVDF-derived samples. On the basis of these observations, we may conclude that the presence of fluorine in the starting materials is required for reduction of Nb(V) under these conditions.

Elemental analysis of the fluorinated compounds is summarized in Table 1. Despite the color changes and structural changes observed in the PVDF-reacted samples, the products contained large amounts of carbon impurity, to the extent that they were enriched in carbon rather than fluorine after the reaction. Treating the samples in multiple grindings with substoichiometric amounts of PTFE produced the best results, which are summarized in Table 1. Some carbonaceous residue still remains, and upon heating the pellet at 600 °C, XRD showed the appearance of extra peaks that could be assigned to graphite fluoride.

On the basis of the total amount of fluorine and carbon present in the samples, we may estimate the fluorine content of the oxide. At one extreme, all of the fluorine is in the layered perovskite compound and the carbon is present as a graphitic phase; the more pessimistic assumption is that all the carbon is present as CF (the terminal composition for graphite fluoride) and only the remaining fluorine is in the oxyfluoride perovskite phase. The smaller the carbon contaminant is, the smaller the uncertainty in $x$ in the formula $RbLaNb_2O_{7-x}F_x$. As shown in Table 1, samples treated twice with 0.6 equiv of PTFE have a fluorine content such that $x \approx 0.5-0.7$, whereas after three such cycles, $x = 0.86-1.3$. Hence, we can approximate the compositions of these products as $RbLaNb_2O_{6.4}F_{0.6}$ and $RbLaNb_2O_6F$. Attempts were made to remove the excess carbon by treatment at 400 °C in air for 12 h; however, a white product was obtained,

(25) Larson, A. C.; Von Dreele, R. B. *General Structure Analysis System (GSAS)*; Report LAUR 86-748; Los Alamos National Laboratory: Los Alamos, NM, 2000.
(26) Toby, B. H. *J. Appl. Crystallogr.* **2001**, *34*, 210–213.
(27) Blaha, P.; Schwarz, K.; Madsen, G. K. H.; Kvasnicka, D.; Luitz, J. *WIEN2k, An Augmented Plane Wave + Local Orbitals Program for Calculating Crystal Properties*; Techn. Universität Wien: Vienna, Austria, 2001; ISBN 3-950131-1-2.
(28) Gomez-Romero, P.; Palacin, M. R.; Casan, N.; Fuertes, A. *Solid State Ionics* **1993**, *63−65*, 424–428.

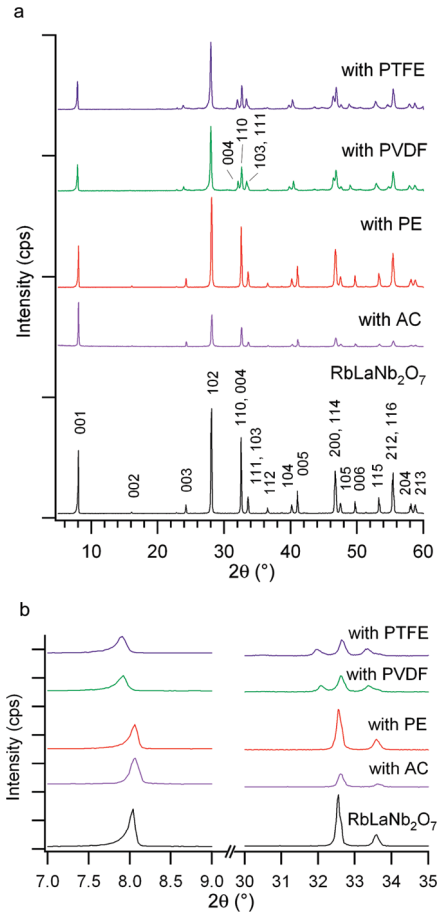


***Figure 3.*** (a) XRD patterns of $RbLaNb_2O_7$ and reaction products. PTFE = poly(tetrafluoroethylene), PVDF = poly(vinylidene fluoride), PE = polyethylene, AC = activated carbon. (b) An expanded view of the low angle region and the region of the 110, 004, 111, and 103 reflections. Reaction of 1.2 and 0.6 equiv of fluoropolymer gave similar results.

***Table 1.*** Elemental Analysis (C, F) Results for Fluorinated Product Mixtures

| sample[a] | C wt % | F wt % | C/F ratio | $F_x$[b] |
|---|---|---|---|---|
| $RbLaNb_2O_7$ + 0.6 equiv, ×2 | 0.44 | 2.44 | 0.29 | 0.5−0.7 |
| $RbLaNb_2O_7$ + 0.6 equiv, ×3 | 0.93 | 4.44 | 0.33 | 0.86−1.3 |
| $KCa_2Nb_3O_{10}$ + 0.5 equiv, ×3 | 0.67 | 2.07 | 0.53 | 0−0.6 |

[a] All reactions with PTFE. [b] $F_x$ is the analytical fluorine content according to the chemical formula $RbLaNb_2O_{7-x}F_x$ or $KCa_2Nb_3O_{10-x}F_x$.

indicating the oxidation of Nb and loss of mixed valency. The C/F ratios for fluorinated perovskites other than $RbLaNb_2O_{7-x}F_x$ were higher, and thus Rietveld analysis and transport studies focused on this $n = 2$ compound.

**Structural Changes.** Table 2 compares the unit cell parameters of various oxyfluoride products. Fluorination of $RbLaNb_2O_7$ resulted in a unit cell with a longer *c* axis but a *smaller a* parameter, with more distortion resulting at higher degrees of fluorination. Fluorination of $NaYTiO_4$ led to an increased *c* parameter (from 12.21 to 12.95 Å), and the *a*, *b* parameters also increased somewhat. The $n = 3$ compound $KCa_2Nb_3O_{10}$ showed a much smaller structural change under the same reaction conditions despite a similar color change. The general trend is that the changes in unit cell dimensions are smaller with increasing number of layers in the perovskite blocks. $RbLaTiNbO_6F$ and $RbSrNb_2O_6F$ are previously reported Nb(V) oxyfluoride Dion−Jacobson phases that are structurally very similar to $RbLaNb_2O_6F$ prepared in this study. The lattice

***Table 2.*** Lattice Parameters of Layered Perovskite Oxides and Oxyfluorides

| | space group | *a* (Å) | *b* (Å) | *c* (Å) | *V* (Å$^3$) |
|---|---|---|---|---|---|
| $RbLaNb_2O_7$[29] | *P4/mmm* | 3.885(2) | 3.885(2) | 10.989(3) | 165.86 |
| $RbLaNb_2O_7$[30] | *P4/mmm* | 3.896(9) | 3.896(9) | 11.027(2) | 167.38 |
| $RbLaNb_2O_7$ (this work) | *P4/mmm* | 3.89170(9) | 3.89170(9) | 11.0072(4) | 166.71 |
| $RbLaNb_2O_{6.4}F_{0.6}$ | *P4/mmm* | 3.87650(14) | 3.87650(14) | 11.1916(7) | 168.18 |
| $RbLaNb_2O_6F$ | *P4/mmm* | 3.86575(16) | 3.86575(16) | 11.2135(7) | 167.58 |
| $RbSrNb_2O_6F$[31] | *P4/mmm* | 3.850 | 3.850 | 11.284 | 167.26 |
| $RbLaTiNbO_6F$[32] | *P4/mmm* | 3.860(1) | 3.860(1) | 10.980(3) | 163.60 |
| $NaYTiO_4$[33] | *Pbcm* | 12.2134(3) | 5.3517(3) | 5.3509(3) | 349.75 |
| $NaYTiO_{4-x}F_x$ | *Pbcm* | 12.9439(21) | 5.3858(9) | 5.3658(7) | 374.07 |
| $KCa_2Nb_3O_{10}$[34] | *Cmcm* | 3.8802(9) | 29.508(6) | 7.714(1) | 883.42 |
| $KCa_2Nb_3O_{10-x}F_x$ | *Cmcm* | 3.8709(4) | 29.5676(32) | 7.7064(9) | 882.02 |

parameters match well with those of $RbSrNb_2O_6F$, notably the shortened *a*-axis and elongated *c*-axis dimensions of the unit cell.

It is difficult to determine which lattice sites are occupied by F atoms, since the X-ray and neutron scattering factors for oxygen and fluorine are very close to each other. As mentioned above, for the $n = 2$ $RbLaNb_2O_{7-x}F_x$ compound, there are three possibilities, namely the central O1 position, the equatorial O2 position, and the apical O3 position (see Figure 1d). In general, fluorine atoms do not occupy the apical O3 site in oxyfluorides of this type, since the shorter Nb−O3 has more covalent character than the other Nb−O bonds. For example, in their study of $KSrNb_2O_6F$ (*Immm*), Yoo *et al*. concluded, on the basis of bond sum valence calculations, that F atoms occupy the equatorial O2 position.[35] In their $RbLaTiNbO_6F$ compound, Caruntu *et al*. refined the structure with F atoms placed at the O1 and O2 sites.[32] Choy *et al*. studied $RbSrNb_2O_6F$ and, from $^{19}F$ NMR and lattice energy calculations, concluded that the F atoms are distributed over the central and equatorial sites (O1, O2).[31]

While these models all assume that fluorine substitutes for oxygen in the perovskite blocks, there are other possibilities in the case of reductive fluorination, notably the replacement of one oxide ion by two fluoride ions, with one of the fluoride ions occupying an interstitial lattice site. This substitution would not involve reduction of B-site cations and would be expected to increase the volume of the unit cell. From Table 2, we can conclude that this substitution reaction is not important for the Dion−Jacobson phase perovskites, because the unit cell volume does not change significantly after fluorination. However, for

(29) Gopalakrishnan, J.; Bhat, V. *Mater. Res. Bull.* **1987**, *22*, 413–417.
(30) Kodenkandath, T. A.; Lalena, J. N.; Zhou, W. L.; Carpenter, E. E.; Sangregorio, C.; Falster, A. U.; Simmons, W. B.; O'Connor, C. J.; Wiley, J. B. *J. Am. Chem. Soc.* **1999**, *121*, 10743–10746.
(31) Choy, J. H.; Kim, J. Y.; Kim, S. J.; Sohn, J. S.; Han, O. H. *Chem. Mater.* **2001**, *13*, 906–912.
(32) Caruntu, G.; Spinu, L.; Wiley, J. B. *Mater. Res. Bull.* **2002**, *37*, 133–140.
(33) Toda, K.; Kameo, Y.; Kurita, S.; Sato, M. *J. Alloys Compd.* **1996**, *234*, 19–25.
(34) Fukuoka, H.; Isami, T.; Yamanaka, S. *J. Solid State Chem.* **2000**, *151*, 40–45.
(35) Yoo, C.-Y.; Kun-Pyo, H.; Kim, S.-J. *Acta Crystallogr., C* **2007**, *63*, 63–65.
(36) Kramer, B.; MacKinnon, A. *Rep. Prog. Phys.* **1993**, *56*, 1469–1564.
(37) Lee, P. A.; Ramakrishnan, T. V. *Rev. Mod. Phys.* **1985**, *57*, 287–337.
(38) Mott, N. *Conduction in Non-Crystalline Materials*; Oxford University Press: Oxford, 1987.
(39) Efros, A. L.; Shklovskii, B. I. *J. Phys. C: Solid State Phys.* **1975**, *8*, L49.
(40) Beutler, D. E.; Giordano, N. *Phys. Rev. B* **1988**, *38*, 8–19.
(41) Hurd, C. M. *J. Phys. C: Solid State Phys.* **1985**, *18*, 6487–6499.

***Table 3.*** Comparison of Total Electronic Energies and Lattice Energies for Compounds with Different Fluorine Atom Distributions[a]

| | F site | total energy (Ry/cell) | total energy (relative) (kJ/mol) | lattice energy (kJ/mol) |
|---|---|---|---|---|
| $RbLaNb_2O_6F$ | O1 (100%) | −39344.3354 | −2899.67 | |
| | O2 (25%) | −39341.1174 | +1324.3 | |
| | O3 (50%) | −39342.1263 | 0 | |
| $RbSrNb_2O_6F$ | O1 (100%) | −28708.740354 | | 4211.904 |
| | O2 (25%) | −28705.453859 | | 4148.496 |
| | O3 (50%) | −28706.466701 | | 2864.88 |

[a] The multiplicities of sites O1, O2, and O3 are 1, 4, and 2 respectively, resulting in the partial filling of the O2 and O3 sites by fluorine.

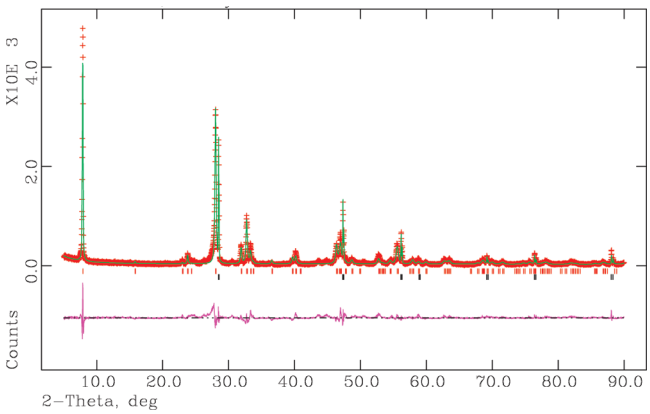


***Figure 4.*** Rietveld refinement of $RbLaNb_2O_6F$. The red tics at the top indicate Bragg reflections of the product phase, and black tics indicate Bragg reflections of silicon powder (internal standard).

$NaYTiO_4$ the unit cell volume increases by about 7%, suggesting that some of the fluoride ions may occupy interstitial sites.

For $RbLaNb_2O_6F$, we performed electronic structure calculations to compare the total electronic energies of structures with the fluorine distributed over the various oxygen sites (Table 3). The different fluorine distributions have very large energy differences: each site distribution differs in energies by 2000−3000 kJ/mol. In contrast, Choy *et al*. found their different fluorine distributions in $RbSrNb_2O_6F$ to differ by only 60−1000 kJ/mol.[31] The reason for this discrepancy is unknown. Total energy calculations were conducted using Rietveld parameters rather than optimized structures, but calculations on $RbLaNb_2O_7$ with the unit cell dimensions of the fluorinated products unit cell yielded a similar result. In comparing the relative stabilities of the $RbLaNb_2O_6F$ structures, we find fluorine at O1 to be the most stable case (as found for $RbSrNb_2O_6F$); the next most stable site, however, is O3, and then O2. Total electronic energy calculations on Choy's $RbSrNb_2O_6F$ also result in the same stability order (also with large energies separating the distributions), so the disagreement is systematic.

Rietveld refinement results for $RbLaNb_2O_7$, $RbLaNb_2O_{6.4}F_{0.6}$, and $RbLaNb_2O_6F$ are given in Figure 4. All samples were refined using the tetragonal *P*4/*mmm* space group, and detailed results are available in the Supporting Information. Electron diffraction of $RbLaNb_2O_6F$ indicated that a $4a \times 4a$ superstructure may be present, but no superstructure peaks could be found in the XRD patterns. In all three samples, the $NbO_6$ octahedra are distorted such that the Nb−O1 bond is longer than the other bonds and the octahedron is "puckered" so that the Nb atom and the equatorial O2 atoms are not coplanar (see Table 4 for selected bond lengths and angles). Although the Rietveld refinements do not give exceptionally good fits,

***Table 4.*** Selected Bond Lengths (Å) of $RbLaNb_2O_7$ and Related Oxyfluorides

| | $RbLaNb_2O_7$ | $RbLaNb_2O_{6.4}F_{0.6}$ | $RbLaNb_2O_6F$ | $RbSrNb_2O_6F$ |
|---|---|---|---|---|
| $d_{apex}$ | 1.770 | 1.821 | 1.693 | 1.726 |
| $d_{center}$ | 2.274 | 2.319 | 2.334 | 2.361 |
| $d_{eqt}$ | 2.016 | 1.983 | 1.996 | 1.988 |
| distortion (°) | 149.6 | 155.7 | 151.2 | 154.1 |

fluorination seems to decrease the distortion angle (defined as O2−Nb−O2), a trend followed by $RbSrNb_2O_6F$. Refinements were also conducted with vacancies at the various oxygen sites, but these failed to give meaningful results, as the occupancy factor for some of the oxygen sites converged at values above 1. The thermal parameters for all atoms were fixed at 0.025 $Å^2$ regardless of site or atom, since fitting yielded slightly negative factors on the oxygen atoms.

**Electronic Structure.** The calculated density of states for $RbLaNb_2O_6F$ with F at the O1 position is shown in Figure 5; the densities of states for the other possible configurations of $RbLaNb_2O_6F$ are qualitatively the same and are included in the Supporting Information, together with that of $RbLaNb_2O_7$. The Fermi level is indicated by the dotted line at 0 eV. Reductive fluorination injects an electron into the conduction band, moving the Fermi level approximately 1 eV above the original band gap (at −4 to −1 eV). Closer examination in the Nb and F1, O2, O3 partial densities of states shows that the conduction band is formed by hybridization of orbitals from Nb and O2, both of which lie in the same plane. The third plot in Figure 5 reveals that the Nb 4d band, which is responsible for conduction, is the $4d_{xy}$ band (blue trace, third pane of Figure 5). This is again coplanar with Nb and O2. The result is a 2-D metallic compound. In general, 2-D metallicity would be expected for any fluorinated layered $d^x$ system where $d = 0-1$; hence, fluorination yields a convenient pathway for transforming the insulating layered perovskites into 2-D metallic conductors. Tobias *et al*. also mention this as the general case,[14] and most $n = 2$ Ruddlesden−Popper and Dion−Jacobson phases are

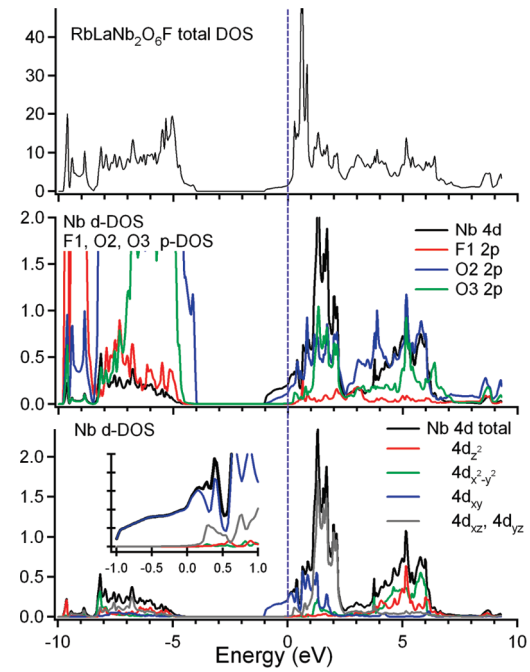


***Figure 5.*** Calculated density of states for $RbLaNb_2O_6F$ (F atoms at the O1 position).

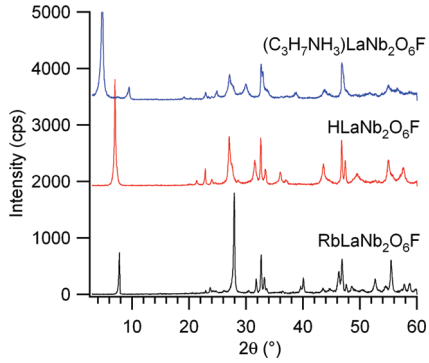


***Figure 6.*** XRD patterns of $RbLaNb_2O_6F$ and ion-exchanged products.

expected to have 2-D metallic behavior. It is possible, however, that disorder of oxygen and fluorine may cause electron localization, resulting in a thermally activated semiconductor, and the virtual crystal approximation (calculations conducted here) would not account for this. The fact that the multiplicity of the O1 site is unity would eliminate the possibility of O−F disorder if the fluorine atoms occupied only the O1 site. However, as noted above, it is likely that F atoms occupy both the O1 and O2 sites.

**Ion Exchange/Exfoliation.** The layered perovskites $RbLaNb_2O_7$ and $KCa_2Nb_3O_{10}$ react with aqueous acid to yield the proton-exchanged products $HLaNb_2O_7$ and $HCa_2Nb_3O_{10}$, which then provide an entry point to exfoliation and layer-by-layer assembly through intercalation of bulky cations. The oxyfluoride $RbLaNb_2O_6F$ is also ion-exchangeable. Figure 6 shows that, after acid treatment, the 00*l* peak at 7.8° shifts to 7.5° ($d_{001}$ = 11.8 Å). The increase in interlayer spacing with the exchange of a smaller cation $H^+$ is probably due to hydrated protons in the interlayer. The product in suspension and after isolation as a dry powder has the same black color of the Rb precursor. Further treatment with a propylamine solution in tetrahydrofuran expanded the interlayer spacing to 18.5 Å, and again a black powder was recovered. Intercalation of ethylamine resulted in a stable dark colloid (see Supporting Information), which presumably consists of exfoliated $LaNb_2O_6F^-$ sheets.

A $RbLaNb_2O_6F$ sample that was proton-exchanged in 2 M HCl for 3 days was found to be approximately 80% exchanged by energy-dispersive spectrometry, and fluorine analysis gave 4.14% F, in excellent agreement with the formulation $Rb_{0.2}H_{0.8}LaNb_2O_6F$ (4.15% F). A pressed pellet of this product had the same DC resistivity ($7 \times 10^2$ Ω·cm) as the original $RbLaNb_2O_6F$ sample. Different preparations of $RbLaNb_2O_6F$ gave resistivities in the range $2-7 \times 10^2$ Ω·cm (see below). The retention of lattice fluorine and electronic conductivity is strong evidence that Nb(IV) in the perovskite blocks is not oxidized, even after exchange with acid and exposure to oxygen from the air for 3 days. This stability is remarkable compared to that of mixed-valent Nb perovskites made by intercalation of alkali metals. A sample that was reacted for 5 days in 2 M nitric acid showed several orders of magnitude higher resistivity, consistent with oxidation of Nb(IV) to Nb(V) after prolonged exposure to acid and oxygen.

**Electronic Transport.** The potential effect of the carbon impurity (approximately 1 wt %) on the electronic conductivity of $RbLaNb_2O_6F$ was examined in a series of control experiments. Pellets of $RbLaNb_2O_6F$, $RbLaNb_2O_7$, and $RbLaNb_2O_7$ containing 1 wt % of graphite were prepared. The respective room-temperature resistivities of the pellets were 195 Ω·cm, >3.4 MΩ·cm, and >2.0 MΩ·cm. Thus, the effect of the carbon impurity on conductivity is rather small.

Results from temperature-dependent resistivity measurements on $RbLaNb_2O_6F$ are shown in Figure 7. Instead of metallic behavior, semiconducting behavior was observed. To understand the mechanisms of conduction, the data were analyzed by fitting to various models, namely Arrhenius-type behavior, Mott variable-range hopping (VRH) behavior in 2-D and 3-D

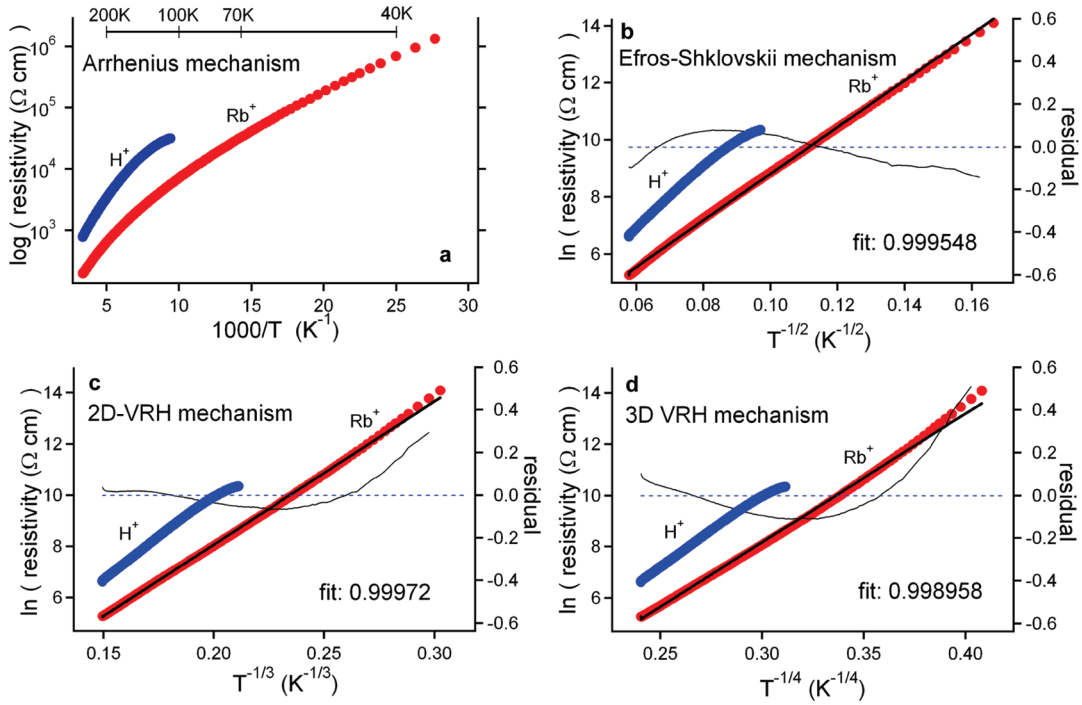


***Figure 7.*** Temperature-dependent resistivity measurements on $RbLaNb_2O_6F$ and $H_{0.8}Rb_{0.2}LaNb_2O_6F$ plotted according to the (a) Arrhenius, (b) Efros−Shklovskii, (c) 2-D Mott variable range hopping, and (d) 3-D Mott variable range hopping mechanisms.

disordered systems,[36−38] and the Coulomb gap model of Efros−Shklovskii (ES), in which there are strong e−e Coulomb interactions.[39] All three models have a similar form, eq 1,

$$\rho = \rho_0 \exp\left(\frac{T_0}{T}\right)^{1/(d+1)} \quad (1)$$

where $\rho$ is the resistivity. In the Arrhenius model, $d = 0$, meaning that there is a fixed activation energy ($kT_0$) as in a typical semiconductor. For the ES Coulomb gap model, $d = 1$ (in both 2-D and 3-D systems), and for the 2-D and 3-D VRH models, $d = 2$ and 3, respectively. In a disordered system with strong localization, $T_0$ is related to a combination of the density of states at the Fermi energy and the localization length; for the ES model, it is also dependent on the dielectric coefficient of the material. Of these models, the thermally activated Arrhenius model with a fixed energy gap is obviously inadequate (Figure 7a). In contrast, all three strong localization models gave reasonable fits, with extremely good fits obtained for the Mott 2-D VRH and ES models. These results suggest strong disorder. This disorder may be structural and is also likely to be occupational, in terms of O/F distributions. The linear fits enable calculation of $T_0$, with $T_{0,ES} = 6.68 \times 10^3$ K and $T_{0,2D\text{-}VRH} = 1.76 \times 10^5$ K. The possibility of a low-temperature crossover between ES and 2-D VRH behavior was investigated, but it is difficult to discern any such transition on the basis of these data. Magnetoresistivity (MR) and voltage−current ($V-I$) measurements were also carried out. An interesting negative magnetoresistance and a linear $V-I$ characteristic behavior were found. At present, we do not have a good explanation for these results (see Supporting Information). For comparison purposes, data fits to 2-D/3-D weak localization[37,40] and models of quantum tunneling through a thermally vibrating barrier[40] are also included in the Supporting Information.

Previous studies have shown that layered perovskites oxides can exhibit a host of electronic behaviors. At high dopant levels, lithiated $KLaNb_2O_7$ has been reported to be metallic, while at lower dopant levels it shows 2-D VRH behavior at 0.5−120 K.[42] $Rb_2LaNb_2O_7$ has been synthesized by reductive intercalation of rubidium vapor, but its transport properties have not yet been measured.[19] Other reduced niobates such as $KCa_{2-x}La_xNb_3O_{10}$ and $RbCa_2Na_{1-x}Sr_xNb_4O_{13}$ have been reported to show quantum tunneling behavior (temperatures of 20−80 and 80−230 K, respectively), although the authors did not examine the possibility of a 2-D VRH mechanism.[21,22] Quantum tunneling has also been reported in $Na_{1-x+y}Ca_{x/2}LaTiO_4$ (80−280 K),[43] while $Na_{2-x+y}Ca_{x/2}La_2Ti_3O_{10}$ exhibits 3-D VRH behavior below 10 K.[43]

## Conclusion

Reductive fluorination using a PTFE is a viable route to obtaining mixed valency in various layered perovskites. Although structural disorder is an inherent obstacle to achieving metallic conductivity, it may be possible to achieve metallic conductivity in these compounds at higher doping levels, and some interesting transport and phase behavior might be expected near the metal−insulator transition. At the doping level of one Nb(IV) atom per formula unit, $RbLaNb_2O_6F$ already possesses substantial electronic conductivity at ambient temperature. Given the relatively low reaction temperature (400 °C) of reductive fluorination using PTFE, this reaction could provide a useful route to mixed valency in many $d^0$ transition metal oxides.

**Acknowledgment.** This work was supported by the National Science Foundation under grant CHE-0910513. Electron microscopy was supported in part by the Pennsylvania State University Materials Research Institute NanoFabrication Network under National Science Foundation Cooperative Agreement No. 0335765, National Nanotechnology Infrastructure Network, with Cornell University.

**Supporting Information Available:** Rietveld refinement results for $RbLaNb_2O_7$, $RbLaNb_2O_{6.4}F_{0.6}$, and $RbLaNb_2O_6F$; selected area electron diffraction pattern of $RbLaNb_2O_{7-x}F$; calculated densities of states of $RbLaNb_2O_7$ and $RbLaNb_2O_6F$ with F at the O2 and O3 positions; photograph of $HLaNb_2O_6F$ after treatment with ethylamine; and additional temperature-dependent resistivity plots, $V-I$ curves, and magnetoresistivity measurements on $RbLaNb_2O_6F$. This material is available free of charge via the Internet at http://pubs.acs.org.

JA9040829

(42) Takano, Y.; Takayanagi, S.; Ogawa, S.; Yamadaya, T.; Mori, N. *Solid State Commun.* **1997**, *103*, 215–217.
(43) Lalena, J. N.; Mcintyre, R. A.; Cushing, B. L.; Thomas, K. A.; Heintz, J. L. J.; Seip, C. T.; O'Connor, C. J.; Wiley, J. B. *Mater. Res. Soc. Symp. Proc.* **1999**, *547*, 99–104.